PROCEEDINGS OF SCIENCE

Reconstruction of muon number of air showers with the surface detector of the Pierre Auger Observatory using neural networks

Steffen Traugott Hahn[a,*] **for the Pierre Auger Collaboration**[b]

[a] *Karlsruhe Institute of Technology KIT, Institute for Astroparticle Physics, Karlsruhe, Germany*

[b] *Observatorio Pierre Auger, Av. San Martín Norte 304, 5613 Malargüe, Argentina*

Full author list: https://www.auger.org/archive/authors_icrc_2023.html

E-mail: spokespersons@auger.org

To understand the physics of cosmic rays at the highest energies, it is mandatory to have an accurate knowledge of their mass composition. Since the mass of the primary particles cannot be measured directly, we have to rely on the analysis of mass-sensitive observables to gain insights into this composition. A promising observable for this purpose is the number of muons at the ground relative to that of an air shower induced by a proton primary of the same energy and inclination angle, commonly referred to as the relative muon number R_μ.

Due to the complexity of shower footprints, the extraction of R_μ from measurements is a challenging task and intractable to solve using analytic approaches. We, therefore, reconstruct R_μ by exploiting the spatial and temporal information of the signals induced by shower particles using neural networks. Using this data-driven approach permits us to tackle this task without the need of modeling the underlying physics and, simultaneously, gives us insights into the feasibility of such an approach.

In this contribution, we summarize the progress of the deep-learning-based approach to estimate R_μ using simulated surface detector data of the Pierre Auger Observatory. Instead of using single architecture, we present different network designs verifying that they reach similar results. Moreover, we demonstrate the potential for estimating R_μ using the scintillator surface detector of the AugerPrime upgrade.

The 38th International Cosmic Ray Conference (ICRC2023)
26 July – 3 August, 2023
Nagoya, Japan

*Speaker

PoS(ICRC2023)318

1. Introduction

Up to date, ultra-high energy cosmic rays (UHECRs) are the most energetic particles observed in our Universe. As they are naturally accelerated, a deeper understanding of them gives us insights into the most extreme processes in our Universe. However, even after decades of research, their exact origin remains elusive [1]. To shed light on this mystery, it is essential to estimate the masses of UHECRs arriving at Earth on a particle-by-particle basis.

Above 10^{16} eV, the direct detection of UHECRs is unfeasible due to their scarcity [2]. Indirect methods work by observing parts of the particle cascades induced by the interaction of UHECRs with air molecules. We will refer to the particle cascades as air showers. An intriguing quantity directly correlated to the mass of the impinging UHECR is the number of muons N_μ produced during the shower. Since the lifetime of the muons is long compared to that of the shower process most of them reach ground level.

The Pierre Auger Observatory is Earth's largest cosmic ray detector designed to measure air showers using the atmosphere as a calorimeter [3]. The observatory follows a hybrid detector concept using (low-uptime) Fluorescence Detectors (FD) to measure the longitudinal evolution of air showers [4] and a Surface Detector array (SD) to measure the (all-)particle densities at the ground level [5]. The central part of the SD consists of 1660 water-Cherenkov detectors (WCDs) arranged in a regular, triangular grid with a 1500 m spacing. Using air shower events detected by both detector systems allows for a cross-calibration of the SD by using the direct energy measurement of the FD. Since the SD measures the (all-)particle density on ground, the measured time signals contain information about the number of arriving muons N_μ. However, shower-to-shower fluctuations, the non-muonic signals in the WCDs, and the strong degeneracy of the mass with the primary particle energy make the estimation of the muon content non-trivial.

To avoid the need for complex analytical modeling, e.g., [6], it is, hence, reasonable to tackle this task by using neural networks (NNs). NNs have been successfully applied to data simulated for and taken by the Observatory. In Ref. [7], it has been shown that an NN-based approach is able to predict the shower depth of the shower maximum X_{max} from SD measurements. Since X_{max} is also a high-level observable related to the primary particle mass using a similar approach is viable for the muon number. In addition, the Pierre Auger Observatory is currently undergoing an upgrade process [8]. An important part of the upgrade is the addition of surface scintillator detectors (SSDs) to most of the WCDs and the change of the detector electronics. The SSDs have a different response to the various particles as the WCD, allowing for an improved disentanglement between the muonic signal and the remaining parts. NNs are a simple way to test this assumption.

2. Relative muon content

Instead of predicting the unbound quantity of N_μ, which depends on both the primary particle energy and the inclination angle of the shower, we train our networks to predict the relative muon content

$$R_\mu = \frac{N_\mu}{\langle N_\mu^{\mathrm{p}} \rangle}, \tag{1}$$

where $\langle N_\mu^{\mathrm{p}} \rangle$ is the expected number of muons for an equivalent shower induced by a proton primary of the same primary particle energy E and shower inclination angle θ. The definition in Eq. (1) is motivated by the Heitler-Matthews model for hadronic air showers [9]: under the assumption that only pions are produced during hadronic interactions, $R_\mu \propto A^{1-\delta}$, where δ is a small positive constant.

To train NNs we use air showers simulated with CORSIKA [10] using the hadronic interaction model EPOS-LHC [11]. For the supervised training of NNs, we require labels for our detected shower footprints. However, the exact number of muons at ground-level N_μ is not directly accessible due to cuts near the shower core. Therefore, we use the total number of (anti-)muons at the shower depth X of the observatory at ground-level found in the simulation files. We denote this proxy as N_μ^{C}.

To compute R_μ from N_μ^{C}, we need $\langle N_\mu^{\mathrm{p}} \rangle$ for all primary particle energies E and all shower inclination angles θ. We parameterize the expected value for air showers induced by a proton primary via

$$\langle N_\mu^{\mathrm{p}} \rangle(E, \theta) = f(\theta)\, 10^{A + B \lg E} = [a + bx + cx^2 + dx^3]\, 10^{A + B \lg E}, \tag{2}$$

where $x = \sin^2 \theta$ and the set $\{a, b, c, A, B\}$ are fit parameters. The dependence of $\langle N_\mu^{\mathrm{p}} \rangle$ on the primary particle energy is stronger than that on the inclination angle. Therefore, we perform a two-step fit to estimate the parameters in Eq. (2). First, we estimate $\langle \lg N_\mu^{\mathrm{p}} \rangle(E)$ by fitting solely the exponent in Eq. (2). We then fit the remaining $\{a, b, c\}$ by fixing $\{A, B\}$. Note that the second fit rectifies the error of fitting $\langle \lg N_\mu^{\mathrm{p}} \rangle(E)$ in the first step instead of $\langle N_\mu^{\mathrm{p}} \rangle$.

The main goal of constructing and subsequently predicting R_μ is to use the quantity as an estimate for the primary particle mass A. To assess how good we are able to separate between showers induced by low-mass and high-mass primaries, we consider two metrics. We estimate the separability with the commonly used merit factor between proton and iron events defined as

$$mf = \frac{\left| \langle R_\mu \rangle_{\mathrm{p}} - \langle R_\mu \rangle_{\mathrm{Fe}} \right|}{\sqrt{\sigma_{\mathrm{p}}^2 + \sigma_{\mathrm{Fe}}^2}}, \tag{3}$$

where the subscripts denote that the average and standard deviation is computed for proton (p) and iron (Fe) primaries. The merit factor is a measure of goodness for our final predictor and an estimator of mass separation of air shower events. We supplement this metric using the accuracy of classifying if a shower event has been induced by a light or heavy primary particle.

Baseline models To ensure that an NN-based approach is reasonable, we need to demonstrate its benefits if compared to alternative reference models. Therefore, we want to show that geometric and time signal information play a crucial role in the estimation of R_μ. To exploit this type of information in analytic approaches would require complex model building. We chose a Boosted Decision Tree (BDT) to test a machine learning model that does not have direct access to the geometry and time signals. To do this we flatten[1] the non-time-signal inputs which are given to the advanced NN models and add two additional hand-selected features extracted from the traces of each detector (see Sec. 3). To show that the addition of geometric information improves the situation, but is not sufficient, we use an alternative yet simpler NN-based model, denoted as ALT. The ALT model uses the unflattened inputs of the BDT to predict R_μ.

[1] We make a copy of a multidimensional array collapsed into one dimension.

Base data set Our shower data set consists of 88 161 CORSIKA simulations using the hadronic interaction model EPOS-LHC. The data set contains air showers induced by proton, Helium, Oxygen, and Iron primaries in equal proportions. The simulated air showers are uniformly distributed in $\lg(E/\mathrm{eV})$ in the interval $[10^{18}\,\mathrm{eV}, 10^{20.2}\,\mathrm{eV}]$ and in $\sin^2\theta$ in the inclination range $[0°, 65°)$. The detector response is simulated using $\overline{\text{Off}}\underline{\text{line}}$ [12]. To increase the amount of training data available, each of the CORSIKA showers is used ten times. From this setup[2], we have obtained 816 571 events for Phase-I simulations (old electronics, only WCD) and 830 491 events for Phase-II simulations (new electronics, WCD and SSD).

3. Neural network based approach

The extraction of the muon content using NNs at the Pierre Auger Observatory falls into two categories, which differ in the use of shower information. The first category of methods uses (mostly) localized information of triggered WCD stations [13] to determine the muon content in a single station. From the muon content of all triggered WCDs in an event, it should be possible to estimate another proxy for N_μ. However, this analysis is beyond the scope of this study. We focus here on the second category of NN-based analyses: the predicting of R_μ from all the information contained in the shower footprint, as has been done in Ref. [7].

Preparation of data. The SD has a triangular grid structure. To transfer the information in the shower footprint into rectangular memory, we follow the encoding procedure described in Ref. [14]. Note that using this procedure also "normalizes" the showers using the reconstructed azimuth angle by reflecting and rotating the shower footprints in such a way that they fall into a 30° azimuth interval. In this way we do not need to use a special architecture to account for the corresponding symmetries. We only encode information from stations that fit into a 5×5 grid of rectangular memory.

We take 3 µs of the time signals in the SD stations and normalize the signals via

$$\hat{S}(t) = \frac{\lg(S(t)/[S] + 1)}{\lg(100 + 1)}, \tag{4}$$

where $S(t)$ is the average of all PMTs of the corresponding detector and $[S]$ is the unit of the signal (VEM for the WCD, MIP for the SSD). Due to the increased sampling rate of the new electronics in Phase-II simulations we average over three successive bins making the signals equivalent to the sampling rate of Phase-I simulations. In addition to the time signal data, we add a "Boolean" map[3] of the triggered stations b_{tr}, the standardized trigger timing information $\hat{t}$, the information whether a station is low-gain saturated b_{LG}, the distance to the shower axis r_{sh}, and the plane front shower time t_{pf} as station-level inputs and the inclination angle $\sin^2\theta$ as an event-level input. The trigger time information $\hat{t}$ is the standard score of t using the average trigger time of the event as mean value $\langle t\rangle$ of the population and the standard deviation over all events as the standard deviation σ of the difference $t - \langle t\rangle$. The distance to the shower axis r_{sh} is the minimum distance from a station

[2] Since parts of the phase space lie outside of the full efficiency of the observatory, the number of shower events is lower than ten times that of the CORSIKA simulations.

[3] We use the floating point values 1.0 and 0.0 for true and false, respectively.

to the shower axis. We normalize it by dividing by 1000 m. The plane front time t_{pf} is the time a plane front would arrive at all stations relative to the arrival at the central station. Adding the plane front time to the trigger time implicitly encodes the curvature of the shower front. For each station-level input an event has one value for each triggered SD station. Since the the inclination angle is a shower observable we fill a 5×5 array of memory with the constant value at the positions of the triggered stations. Thus, for each event the additional input has a size of 5×5×6. For all mentioned, additional inputs, we use reconstructed quantities using the standard reconstructions found in Offline.

Basic network architecture. We build our NNs with the `Python3` bindings of `TensorFlow` 2.12 using only standard layers already implemented in the `TensorFlow` framework. The basic topology of the NN architecture employed consists of two subnetworks denoted as N1 and N2. Since the time signals have a length of 120 time bins, it is unfeasible to directly correlate the spatial information. Therefore, the main purpose of subnetwork N1 is to compress the information in the time signals to n_{f} (auto-)generated features which are useful for predicting R_{μ}. To test the importance of the trace information, we use three distinct sub-architectures for N1. To estimate how much information is used from the traces, we replace N1 with a fixed architecture that extracts the total signal and rise time from the traces. This is the ALT network discussed in the previous section. We compare ALT to a convolution-based (CNN) and LSTM-based (RNN) subnetwork that extract 12 and 16 features, respectively. Using weight-sharing, all subnetworks work independently on each time signal and treat all time signals equally. The inputs $\hat{S}$ of subnetwork N1 can have an arbitrary number of channels if the CNN or RNN architectures are used. Therefore, the only difference for the training and inference of Phase-I and Phase-II data lies in the number of channels given. When SSD information is used, we simply treat it as an additional channel to the already existing WCD channel. The output of N1 is then concatenated to the additional station- and event-level input data (see Sec. 3). For ALT, CNN, and RNN the $(n_{\mathrm{f}} + 6)$ features for each encoded position are then used as input for the second subnetwork N2. N2 is a 2d-convolution-based network that correlates the spatial information in the shower footprint. A final dense layer with one unit yields the scalar output R_{μ}^{pred}. This network architecture also works for other global observables, such as the primary energy E [15] and the shower depth of the shower maximum X_{max}, and is very robust.

Training process. For the NN training, we draw without replacement from the base data set (see Sec. 2). We divide the data set in a training data and test data set. For Phase-I simulations we have 479 879 and 119 970 events, respectively, and in Phase-II simulation we have 479 882 and 119 971 events, respectively During training we use 10% of the training data set as a validation set.

Training NNs in parallel environments is non-deterministic. Therefore, we train ten NNs for each of the different architectures using the same starting conditions. We select the best performing one by comparing the linear correlation of R_{μ}^{true} and R_{μ}^{pred}. Henceforth, we denote their difference as ΔR_{μ} and the standard deviation of ΔR_{μ} as $\sigma_{\Delta R_{\mu}}$. To reduce the bias caused by the degeneracy of mass and energy we use a loss function of the form

$$\mathcal{L}\left(R_{\mu}^{\mathrm{pred}}, R_{\mu}^{\mathrm{true}}\right) = \sum_{x=\mathrm{p},\ldots,\mathrm{Fe}} \left(\left(\sigma_{\Delta R_{\mu}}^{(x)}\right)^2 + \left(\Delta^{(x)} R_{\mu}\right)^2 \right), \tag{5}$$

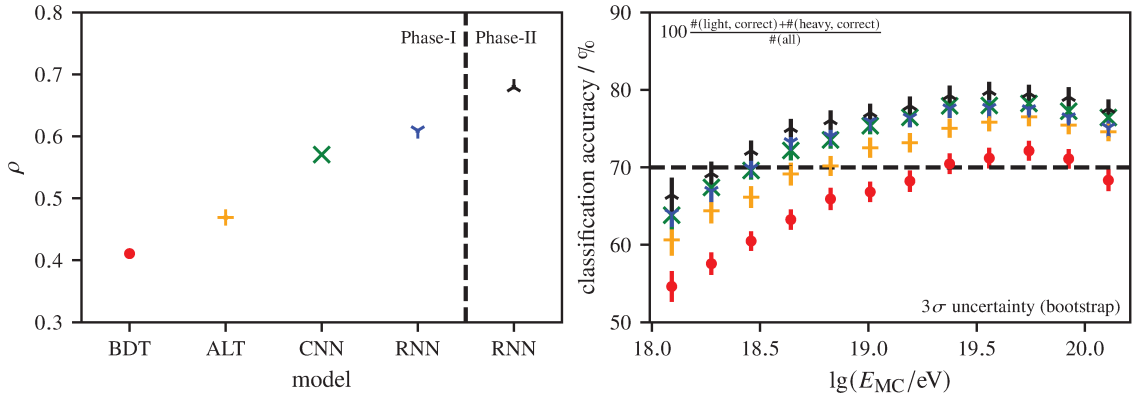

Figure 1: Comparison of the performance of the different models on the test data sets. *Left:* Pearson correlation coefficient of the predictions and true R_μ for the different models over the entire phase space. *Right:* Accuracy of the classification of showers induced by light (proton, Helium) and heavy (Oxygen, Iron) primaries in different energy bins. The 99.7% uncertainty of the accuracies has been estimated using a bootstrap algorithm. Due to the large amount of data in each bin, they are barely visible. The horizontal dashed line is a rough estimate of the performance of the BDT for high energies.

where the superscript (x) indicates that the standard deviation and mean are taken only for the events (in the batch) induced by the primary x. For the training process, we use the Adam optimizer using an initial learning rate of 0.0022. For all training processes the batch size is set to 128 and the maximum number of epochs is set to 80. Training is stopped prematurely if the validation loss does not improve over 5 epochs.

4. Results on simulation data

Comparison of different models. Fig. 1 shows the classification accuracy of events induced by light and heavy primaries in the correlation of R_μ^{true} and R_μ^{pred} for the different models presented in Secs. 2 and 3. According to both metrics the BDT is the worst model barely reaching 70% classification accuracy at the highest energies. The performance of the ALT model demonstrates that the geometric information of the shower footprint is very important for the prediction of R_μ. Both the accuracy and the linear correlation improves compared to the BDT. Using the full WCD signal trace information further improves the separability. Although, the linear correlation of the predictions of RNN are slightly better than that of CNN, this does not affect the accuracy which is very similar. Hence, we expect that even more sophisticated models being able to extract better features from the traces do not necessarily help in the mass separation. The reduced gain might be an indicator that all important information from the time signals of the WCD is already used for the R_μ prediction. Adding the SSD time signals from Phase-II data to the inputs of the RNN model yields another direct improvement in both metrics. The increase in linear correlation and accuracy is similar to that from ALT to the CNN and RNN models.

Performance on Phase-I data. We use the bias $\Delta^{(x)}$ as a measure of precision and the standard deviation $\sigma^{(x)}$ as a measure for accuracy (see Eq. (5)) to evaluate the performance of the best performing model on Phase-I data. Fig. 2 depicts both metrics for all available primaries of the test

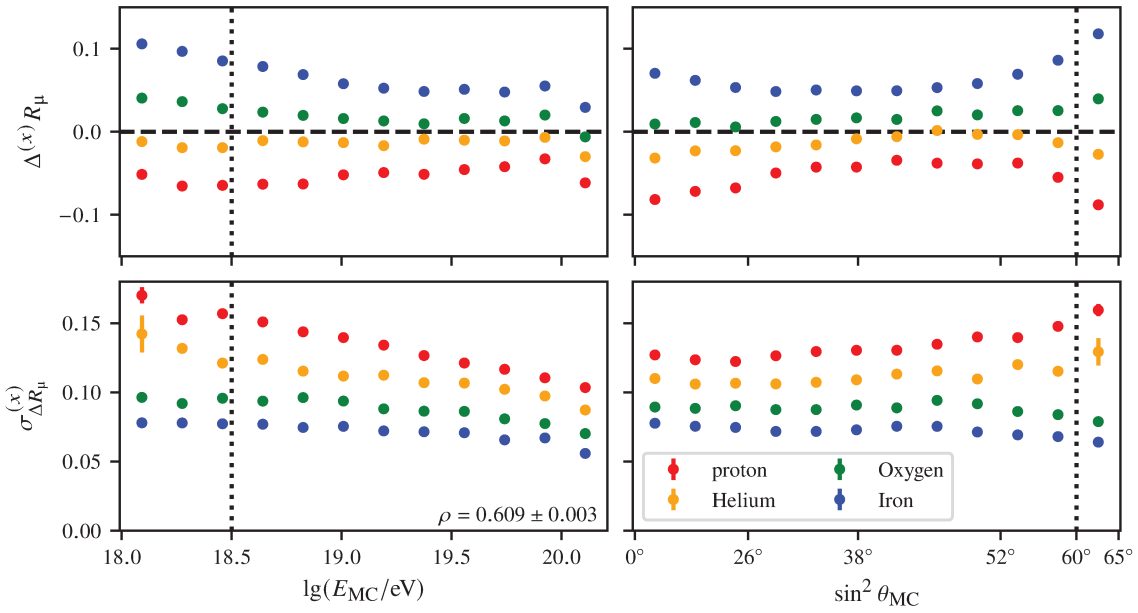

Figure 2: Bias (*top* panels) and resolution (*bottom* panels) of R_μ predictions of the RNN-based NN for each of the available primaries on the Phase-I test data set (see Sec. 3) binned in logarithmic Monte-Carlo energy (*left* panels) and $\sin^2 \theta_{MC}$ (*right* panels). The vertical, dashed black lines depict the minimum energy and maximum inclination angle where the SD array has 100% efficiency. The number in the bottom-right corner of the *bottom-left* panel is the Pearson correlation coefficient ρ for the population of pairs $(R_\mu^{pred}, R_\mu^{true})$. The uncertainty on ρ is the averaged 1σ bootstrap confidence interval.

data set in bins of $\lg(E_{MC}/eV)$ and $\sin^2 \theta_{MC}$. The accuracy of the predictions improves consistently for higher energies for all primaries. This improvement is an effect of the increased number of triggered stations offering more information. The precision remains almost constant after the SD reaches full efficiency at $10^{18.5}$ eV only significantly deviating in the last bin. This deviation is due to the proximity to the edge of the training phase space. For the inclination angle the network predictions are especially precise around 38°. This is the median inclination angle (in terms of solid angle) in the interval $[0°, 60°]$ where the SD is fully efficient.

Phase-I versus Phase-II. As can be seen in Fig. 1, including the SSD information in the inputs increases the correlation between the predictions and the true values of R_μ without the need to adjust the architecture of the RNN. This improvement is even visible in the correlation plots (*left* panels) in Fig. 3. Moreover, adding the SSD also shows an improvement in *mf* (see Eq. (3)) over the entire energy range, even when we use reconstructed energy E^*_{rec} instead of the Monte-Carlo energy E_{MC}.

5. Conclusion

In this contribution, we have shown that it is possible to predict the muon content R_μ of hadronic air showers from shower footprints detected by the SD of the Pierre Auger Observatory using NN-based methods. Moreover, we have demonstrated that spatial and trace information are useful for these predictions. In addition, we have verified that the use of additional information

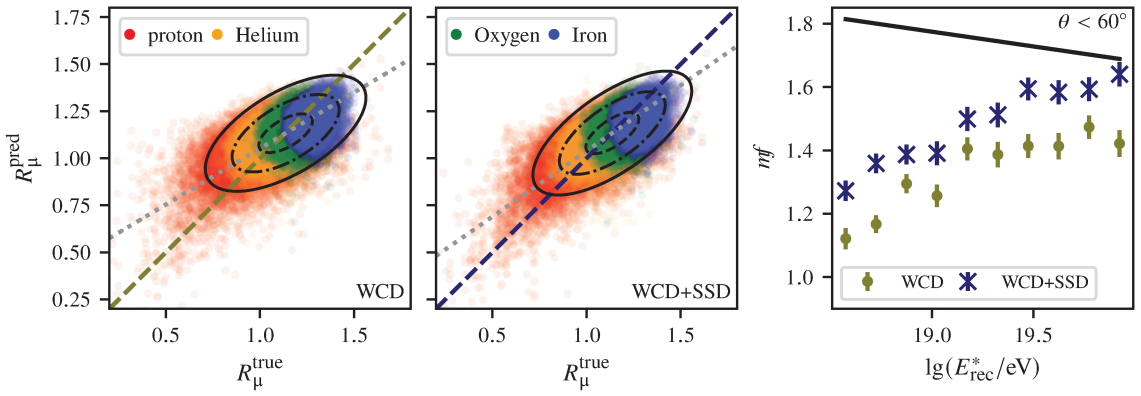

Figure 3: Correlation of R_μ^{true} and R_μ^{pred} (two *left* panels) for the Phase-I (*first* panel) and Phase-II (*second* panel) data sets and comparison of merit factors (see Eq. (3)) of proton and iron predictions for both data sets (*right* panel). In each case, we use data from the phase space for which the SD is fully efficient. The black ellipses in the *left* panels are the 1σ to 3σ bounds assuming a Gaussian distribution. The gray, dotted lines are the straight lines which intersect the major axes of the corresponding ellipses. To compute the merit factors we cut the base data set to the phase space in which the array is fully efficient. The diagonal dashed lines in the two *left* panels are the bisectors. The straight black solid line in the *right* panel is a fit to the binned merit factors if Monte-Carlo energy and R_μ^{true} would be used directly.

given by the SSD improves the prediction of R_μ without requiring any adjustment to the presented methods. This improvement results in a much better separation between light and heavy primary particles even when using reconstructed energies.

Combining the prediction of R_μ with the new methods for predicting X_{max} from the shower footprint will allow for a better estimate of the primary particle masses on an event-by-event basis [16]. This estimate will be further improved by incorporating the new Phase-II data simulated for and taken by the Pierre Auger Observatory. Due to the simplicity of the network architectures used, we also expect that the precision and accuracy of R_μ predictions will further improve when using more complex architectures.

References

[1] R. Alves Batista *et al.*, Front. Astron. Space Sci. **6** (2019) 23.

[2] V. Verzi *et al.* [Pierre Auger]. In 36th International Cosmic Ray Conference **358** (2021) 450.

[3] A. Aab *et al.* [Pierre Auger], Nucl. Instrum. Methods Phys. Res. A **798** (2015) 172–213.

[4] J. Abraham *et al.* [Pierre Auger], Nucl. Instrum. Methods Phys. Res. A **620** (2010) 227–251.

[5] I. Allekotte *et al.* [Pierre Auger], Nucl. Instrum. Methods Phys. Res. A **586** (2008) 409–420.

[6] A. Bridgeman *et al.* [Pierre Auger]. In 35th International Cosmic Ray Conference **301** (2018) 323.

[7] A. Aab *et al.* [Pierre Auger], J. Instrum. **16** (2021) P07019.

[8] A Aab. *et al.* [Pierre Auger], arXiv **1604.03637** (2016).

[9] J. Matthews, Astropart. Phys. **22** (2005) 387–397.

[10] D. Heck *et al.*, Report FZKA **6019** (1998).

[11] T. Pierog *et al.*, Phys. Rev. C **92** (2015) 034906.

[12] S. Argiro *et al.*, Nucl. Instrum. Methods Phys. Res. A **580** (2007) 1485–1496.

[13] A. Aab *et al.* [Pierre Auger], J. Instrum. **16** (2021) P07016.

[14] S. T. Hahn *et al.* [Pierre Auger]. In 37th International Cosmic Ray Conference **395** (2022) 239.

[15] F. Ellwanger *et al.* [Pierre Auger]. In 38th International Cosmic Ray Conference, in these proceedings.

[16] N. Langer *et al.* [Pierre Auger]. In 38th International Cosmic Ray Conference, in these proceedings.

PoS(ICRC2023)318

The Pierre Auger Collaboration

A. Abdul Halim[13], P. Abreu[72], M. Aglietta[54,52], I. Allekotte[1], K. Almeida Cheminant[70], A. Almela[7,12], R. Aloisio[45,46], J. Alvarez-Muñiz[79], J. Ammerman Yebra[79], G.A. Anastasi[54,52], L. Anchordoqui[86], B. Andrada[7], S. Andringa[72], C. Aramo[50], P.R. Araújo Ferreira[42], E. Arnone[63,52], J. C. Arteaga Velázquez[67], H. Asorey[7], P. Assis[72], G. Avila[11], E. Avocone[57,46], A.M. Badescu[75], A. Bakalova[32], A. Balaceanu[73], F. Barbato[45,46], A. Bartz Mocellin[85], J.A. Bellido[13,69], C. Berat[36], M.E. Bertaina[63,52], G. Bhatta[70], M. Bianciotto[63,52], P.L. Biermann[h], V. Binet[5], K. Bismark[39,7], T. Bister[80,81], J. Biteau[37], J. Blazek[32], C. Bleve[36], J. Blümer[41], M. Boháčová[32], D. Boncioli[57,46], C. Bonifazi[8,26], L. Bonneau Arbeletche[21], N. Borodai[70], J. Brack[j], P.G. Brichetto Orchera[7], F.L. Briechle[42], A. Bueno[78], S. Buitink[15], M. Buscemi[47,61], M. Büsken[39,7], A. Bwembya[80,81], K.S. Caballero-Mora[66], S. Cabana-Freire[79], L. Caccianiga[59,49], I. Caracas[38], R. Caruso[58,47], A. Castellina[54,52], F. Catalani[18], G. Cataldi[48], L. Cazon[79], M. Cerda[10], A. Cermenati[45,46], J.A. Chinellato[21], J. Chudoba[32], L. Chytka[33], R.W. Clay[13], A.C. Cobos Cerutti[6], R. Colalillo[60,50], A. Coleman[90], M.R. Coluccia[48], R. Conceição[72], A. Condorelli[37], G. Consolati[49,55], M. Conte[56,48], F. Convenga[41], D. Correia dos Santos[28], P.J. Costa[72], C.E. Covault[84], M. Cristinziani[44], C.S. Cruz Sanchez[3], S. Dasso[4,2], K. Daumiller[41], B.R. Dawson[13], R.M. de Almeida[28], J. de Jesús[7,41], S.J. de Jong[80,81], J.R.T. de Mello Neto[26,27], I. De Mitri[45,46], J. de Oliveira[17], D. de Oliveira Franco[21], F. de Palma[56,48], V. de Souza[19], E. De Vito[56,48], A. Del Popolo[58,47], O. Deligny[34], N. Denner[32], L. Deval[41,7], A. di Matteo[52], M. Dobre[73], C. Dobrigkeit[21], J.C. D'Olivo[68], L.M. Domingues Mendes[72], J.C. dos Anjos, R.C. dos Anjos[25], J. Ebr[32], F. Ellwanger[41], M. Emam[80,81], R. Engel[39,41], I. Epicoco[56,48], M. Erdmann[42], A. Etchegoyen[7,12], C. Evoli[45,46], H. Falcke[80,82,81], J. Farmer[89], G. Farrar[88], A.C. Fauth[21], N. Fazzini[e], F. Feldbusch[40], F. Fenu[41,d], A. Fernandes[72], B. Fick[87], J.M. Figueira[7], A. Filipčič[77,76], T. Fitoussi[41], B. Flaggs[90], T. Fodran[80], T. Fujii[89,f], A. Fuster[7,12], C. Galea[80], C. Galelli[59,49], B. García[6], C. Gaudu[38], H. Gemmeke[40], F. Gesualdi[7,41], A. Gherghel-Lascu[73], P.L. Ghia[34], U. Giaccari[48], M. Giammarchi[49], J. Glombitza[42,g], F. Gobbi[10], F. Gollan[7], G. Golup[1], M. Gómez Berisso[1], P.F. Gómez Vitale[11], J.P. Gongora[11], J.M. González[1], N. González[7], I. Goos[1], D. Góra[70], A. Gorgi[54,52], M. Gottowik[79], T.D. Grubb[13], F. Guarino[60,50], G.P. Guedes[22], E. Guido[44], S. Hahn[39], P. Hamal[32], M.R. Hampel[7], P. Hansen[3], D. Harari[1], V.M. Harvey[13], A. Haungs[41], T. Hebbeker[42], C. Hojvat[e], J.R. Hörandel[80,81], P. Horvath[33], M. Hrabovský[33], T. Huege[41,15], A. Insolia[58,47], P.G. Isar[74], P. Janecek[32], J.A. Johnsen[85], J. Jurysek[32], A. Kääpä[38], K.H. Kampert[38], B. Keilhauer[41], A. Khakurdikar[80], V.V. Kizakke Covilakam[7,41], H.O. Klages[41], M. Kleifges[40], F. Knapp[39], N. Kunka[40], B.L. Lago[16], N. Langner[42], M.A. Leigui de Oliveira[24], Y Lema-Capeans[79], V. Lenok[39], A. Letessier-Selvon[35], I. Lhenry-Yvon[34], D. Lo Presti[58,47], L. Lopes[72], L. Lu[91], Q. Luce[39], J.P. Lundquist[76], A. Machado Payeras[21], M. Majercakova[32], D. Mandat[32], B.C. Manning[13], P. Mantsch[e], S. Marafico[34], F.M. Mariani[59,49], A.G. Mariazzi[3], I.C. Mariş[14], G. Marsella[61,47], D. Martello[56,48], S. Martinelli[41,7], O. Martínez Bravo[64], M.A. Martins[79], M. Mastrodicasa[57,46], H.J. Mathes[41], J. Matthews[a], G. Matthiae[62,51], E. Mayotte[85,38], S. Mayotte[85], P.O. Mazur[e], G. Medina-Tanco[68], J. Meinert[38], D. Melo[7], A. Menshikov[40], C. Merx[41], S. Michal[33], M.I. Micheletti[5], L. Miramonti[59,49], S. Mollerach[1], F. Montanet[36], L. Morejon[38], C. Morello[54,52], A.L. Müller[32], K. Mulrey[80,81], R. Mussa[52], M. Muzio[88], W.M. Namasaka[38], S. Negi[32], L. Nellen[68], K. Nguyen[87], G. Nicora[9], M. Niculescu-Oglinzanu[73], M. Niechciol[44], D. Nitz[87], D. Nosek[31], V. Novotny[31], L. Nožka[33], A Nucita[56,48], L.A. Núñez[30], C. Oliveira[19], M. Palatka[32], J. Pallotta[9], S. Panja[32], G. Parente[79], T. Paulsen[38], J. Pawlowsky[38], M. Pech[32], J. Pękala[70], R. Pelayo[65], L.A.S. Pereira[23], E.E. Pereira Martins[39,7], J. Perez Armand[20], C. Pérez Bertolli[7,41], L. Perrone[56,48], S. Petrera[45,46], C. Petrucci[57,46], T. Pierog[41], M. Pimenta[72], M. Platino[7], B. Pont[80], M. Pothast[81,80], M. Pourmohammad Shahvar[61,47], P. Privitera[89], M. Prouza[32], A. Puyleart[87], S. Querchfeld[38], J. Rautenberg[38], D. Ravignani[7], M. Reininghaus[39], J. Ridky[32], F. Riehn[79], M. Risse[44], V. Rizi[57,46], W. Rodrigues de Carvalho[80], E. Rodriguez[7,41], J. Rodriguez Rojo[11], M.J. Roncoroni[7], S. Rossoni[43], M. Roth[41], E. Roulet[1], A.C. Rovero[4], P. Ruehl[44], A. Saftoiu[73], M. Saharan[80], F. Salamida[57,46], H. Salazar[64], G. Salina[51], J.D. Sanabria Gomez[30], F. Sánchez[7], E.M. Santos[20], E. Santos[32],

F. Sarazin[85], R. Sarmento[72], R. Sato[11], P. Savina[91], C.M. Schäfer[41], V. Scherini[56,48], H. Schieler[41], M. Schimassek[34], M. Schimp[38], F. Schlüter[41], D. Schmidt[39], O. Scholten[15,i], H. Schoorlemmer[80,81], P. Schovánek[32], F.G. Schröder[90,41], J. Schulte[42], T. Schulz[41], S.J. Sciutto[3], M. Scornavacche[7,41], A. Segreto[53,47], S. Sehgal[38], S.U. Shivashankara[76], G. Sigl[43], G. Silli[7], O. Sima[73,b], F. Simon[40], R. Smau[73], R. Šmída[89], P. Sommers[k], J.F. Soriano[86], R. Squartini[10], M. Stadelmaier[32], D. Stanca[73], S. Stanič[76], J. Stasielak[70], P. Stassi[36], S. Strähnz[39], M. Straub[42], M. Suárez-Durán[14], T. Suomijärvi[37], A.D. Supanitsky[7], Z. Svozilikova[32], Z. Szadkowski[71], A. Tapia[29], C. Taricco[63,52], C. Timmermans[81,80], O. Tkachenko[41], P. Tobiska[32], C.J. Todero Peixoto[18], B. Tomé[72], Z. Torrès[36], A. Travaini[10], P. Travnicek[32], C. Trimarelli[57,46], M. Tueros[3], M. Unger[41], L. Vaclavek[33], M. Vacula[33], J.F. Valdés Galicia[68], L. Valore[60,50], E. Varela[64], A. Vásquez-Ramírez[30], D. Veberič[41], C. Ventura[27], I.D. Vergara Quispe[3], V. Verzi[51], J. Vicha[32], J. Vink[83], J. Vlastimil[32], S. Vorobiov[76], C. Watanabe[26], A.A. Watson[c], A. Weindl[41], L. Wiencke[85], H. Wilczyński[70], D. Wittkowski[38], B. Wundheiler[7], B. Yue[38], A. Yushkov[32], O. Zapparrata[14], E. Zas[79], D. Zavrtanik[76,77], M. Zavrtanik[77,76]

———— • ————

[1] Centro Atómico Bariloche and Instituto Balseiro (CNEA-UNCuyo-CONICET), San Carlos de Bariloche, Argentina
[2] Departamento de Física and Departamento de Ciencias de la Atmósfera y los Océanos, FCEyN, Universidad de Buenos Aires and CONICET, Buenos Aires, Argentina
[3] IFLP, Universidad Nacional de La Plata and CONICET, La Plata, Argentina
[4] Instituto de Astronomía y Física del Espacio (IAFE, CONICET-UBA), Buenos Aires, Argentina
[5] Instituto de Física de Rosario (IFIR) – CONICET/U.N.R. and Facultad de Ciencias Bioquímicas y Farmacéuticas U.N.R., Rosario, Argentina
[6] Instituto de Tecnologías en Detección y Astropartículas (CNEA, CONICET, UNSAM), and Universidad Tecnológica Nacional – Facultad Regional Mendoza (CONICET/CNEA), Mendoza, Argentina
[7] Instituto de Tecnologías en Detección y Astropartículas (CNEA, CONICET, UNSAM), Buenos Aires, Argentina
[8] International Center of Advanced Studies and Instituto de Ciencias Físicas, ECyT-UNSAM and CONICET, Campus Miguelete – San Martín, Buenos Aires, Argentina
[9] Laboratorio Atmósfera – Departamento de Investigaciones en Láseres y sus Aplicaciones – UNIDEF (CITEDEF-CONICET), Argentina
[10] Observatorio Pierre Auger, Malargüe, Argentina
[11] Observatorio Pierre Auger and Comisión Nacional de Energía Atómica, Malargüe, Argentina
[12] Universidad Tecnológica Nacional – Facultad Regional Buenos Aires, Buenos Aires, Argentina
[13] University of Adelaide, Adelaide, S.A., Australia
[14] Université Libre de Bruxelles (ULB), Brussels, Belgium
[15] Vrije Universiteit Brussels, Brussels, Belgium
[16] Centro Federal de Educação Tecnológica Celso Suckow da Fonseca, Petropolis, Brazil
[17] Instituto Federal de Educação, Ciência e Tecnologia do Rio de Janeiro (IFRJ), Brazil
[18] Universidade de São Paulo, Escola de Engenharia de Lorena, Lorena, SP, Brazil
[19] Universidade de São Paulo, Instituto de Física de São Carlos, São Carlos, SP, Brazil
[20] Universidade de São Paulo, Instituto de Física, São Paulo, SP, Brazil
[21] Universidade Estadual de Campinas, IFGW, Campinas, SP, Brazil
[22] Universidade Estadual de Feira de Santana, Feira de Santana, Brazil
[23] Universidade Federal de Campina Grande, Centro de Ciencias e Tecnologia, Campina Grande, Brazil
[24] Universidade Federal do ABC, Santo André, SP, Brazil
[25] Universidade Federal do Paraná, Setor Palotina, Palotina, Brazil
[26] Universidade Federal do Rio de Janeiro, Instituto de Física, Rio de Janeiro, RJ, Brazil
[27] Universidade Federal do Rio de Janeiro (UFRJ), Observatório do Valongo, Rio de Janeiro, RJ, Brazil
[28] Universidade Federal Fluminense, EEIMVR, Volta Redonda, RJ, Brazil
[29] Universidad de Medellín, Medellín, Colombia
[30] Universidad Industrial de Santander, Bucaramanga, Colombia

PoS(ICRC2023)318

[31] Charles University, Faculty of Mathematics and Physics, Institute of Particle and Nuclear Physics, Prague, Czech Republic
[32] Institute of Physics of the Czech Academy of Sciences, Prague, Czech Republic
[33] Palacky University, Olomouc, Czech Republic
[34] CNRS/IN2P3, IJCLab, Université Paris-Saclay, Orsay, France
[35] Laboratoire de Physique Nucléaire et de Hautes Energies (LPNHE), Sorbonne Université, Université de Paris, CNRS-IN2P3, Paris, France
[36] Univ. Grenoble Alpes, CNRS, Grenoble Institute of Engineering Univ. Grenoble Alpes, LPSC-IN2P3, 38000 Grenoble, France
[37] Université Paris-Saclay, CNRS/IN2P3, IJCLab, Orsay, France
[38] Bergische Universität Wuppertal, Department of Physics, Wuppertal, Germany
[39] Karlsruhe Institute of Technology (KIT), Institute for Experimental Particle Physics, Karlsruhe, Germany
[40] Karlsruhe Institute of Technology (KIT), Institut für Prozessdatenverarbeitung und Elektronik, Karlsruhe, Germany
[41] Karlsruhe Institute of Technology (KIT), Institute for Astroparticle Physics, Karlsruhe, Germany
[42] RWTH Aachen University, III. Physikalisches Institut A, Aachen, Germany
[43] Universität Hamburg, II. Institut für Theoretische Physik, Hamburg, Germany
[44] Universität Siegen, Department Physik – Experimentelle Teilchenphysik, Siegen, Germany
[45] Gran Sasso Science Institute, L'Aquila, Italy
[46] INFN Laboratori Nazionali del Gran Sasso, Assergi (L'Aquila), Italy
[47] INFN, Sezione di Catania, Catania, Italy
[48] INFN, Sezione di Lecce, Lecce, Italy
[49] INFN, Sezione di Milano, Milano, Italy
[50] INFN, Sezione di Napoli, Napoli, Italy
[51] INFN, Sezione di Roma "Tor Vergata", Roma, Italy
[52] INFN, Sezione di Torino, Torino, Italy
[53] Istituto di Astrofisica Spaziale e Fisica Cosmica di Palermo (INAF), Palermo, Italy
[54] Osservatorio Astrofisico di Torino (INAF), Torino, Italy
[55] Politecnico di Milano, Dipartimento di Scienze e Tecnologie Aerospaziali , Milano, Italy
[56] Università del Salento, Dipartimento di Matematica e Fisica "E. De Giorgi", Lecce, Italy
[57] Università dell'Aquila, Dipartimento di Scienze Fisiche e Chimiche, L'Aquila, Italy
[58] Università di Catania, Dipartimento di Fisica e Astronomia "Ettore Majorana", Catania, Italy
[59] Università di Milano, Dipartimento di Fisica, Milano, Italy
[60] Università di Napoli "Federico II", Dipartimento di Fisica "Ettore Pancini", Napoli, Italy
[61] Università di Palermo, Dipartimento di Fisica e Chimica "E. Segrè", Palermo, Italy
[62] Università di Roma "Tor Vergata", Dipartimento di Fisica, Roma, Italy
[63] Università Torino, Dipartimento di Fisica, Torino, Italy
[64] Benemérita Universidad Autónoma de Puebla, Puebla, México
[65] Unidad Profesional Interdisciplinaria en Ingeniería y Tecnologías Avanzadas del Instituto Politécnico Nacional (UPIITA-IPN), México, D.F., México
[66] Universidad Autónoma de Chiapas, Tuxtla Gutiérrez, Chiapas, México
[67] Universidad Michoacana de San Nicolás de Hidalgo, Morelia, Michoacán, México
[68] Universidad Nacional Autónoma de México, México, D.F., México
[69] Universidad Nacional de San Agustin de Arequipa, Facultad de Ciencias Naturales y Formales, Arequipa, Peru
[70] Institute of Nuclear Physics PAN, Krakow, Poland
[71] University of Łódź, Faculty of High-Energy Astrophysics,Łódź, Poland
[72] Laboratório de Instrumentação e Física Experimental de Partículas – LIP and Instituto Superior Técnico – IST, Universidade de Lisboa – UL, Lisboa, Portugal
[73] "Horia Hulubei" National Institute for Physics and Nuclear Engineering, Bucharest-Magurele, Romania
[74] Institute of Space Science, Bucharest-Magurele, Romania
[75] University Politehnica of Bucharest, Bucharest, Romania
[76] Center for Astrophysics and Cosmology (CAC), University of Nova Gorica, Nova Gorica, Slovenia
[77] Experimental Particle Physics Department, J. Stefan Institute, Ljubljana, Slovenia

PoS(ICRC2023)318

[78] Universidad de Granada and C.A.F.P.E., Granada, Spain
[79] Instituto Galego de Física de Altas Enerxías (IGFAE), Universidade de Santiago de Compostela, Santiago de Compostela, Spain
[80] IMAPP, Radboud University Nijmegen, Nijmegen, The Netherlands
[81] Nationaal Instituut voor Kernfysica en Hoge Energie Fysica (NIKHEF), Science Park, Amsterdam, The Netherlands
[82] Stichting Astronomisch Onderzoek in Nederland (ASTRON), Dwingeloo, The Netherlands
[83] Universiteit van Amsterdam, Faculty of Science, Amsterdam, The Netherlands
[84] Case Western Reserve University, Cleveland, OH, USA
[85] Colorado School of Mines, Golden, CO, USA
[86] Department of Physics and Astronomy, Lehman College, City University of New York, Bronx, NY, USA
[87] Michigan Technological University, Houghton, MI, USA
[88] New York University, New York, NY, USA
[89] University of Chicago, Enrico Fermi Institute, Chicago, IL, USA
[90] University of Delaware, Department of Physics and Astronomy, Bartol Research Institute, Newark, DE, USA
[91] University of Wisconsin-Madison, Department of Physics and WIPAC, Madison, WI, USA

—

[a] Louisiana State University, Baton Rouge, LA, USA
[b] also at University of Bucharest, Physics Department, Bucharest, Romania
[c] School of Physics and Astronomy, University of Leeds, Leeds, United Kingdom
[d] now at Agenzia Spaziale Italiana (ASI). Via del Politecnico 00133, Roma, Italy
[e] Fermi National Accelerator Laboratory, Fermilab, Batavia, IL, USA
[f] now at Graduate School of Science, Osaka Metropolitan University, Osaka, Japan
[g] now at ECAP, Erlangen, Germany
[h] Max-Planck-Institut für Radioastronomie, Bonn, Germany
[i] also at Kapteyn Institute, University of Groningen, Groningen, The Netherlands
[j] Colorado State University, Fort Collins, CO, USA
[k] Pennsylvania State University, University Park, PA, USA

Acknowledgments

The successful installation, commissioning, and operation of the Pierre Auger Observatory would not have been possible without the strong commitment and effort from the technical and administrative staff in Malargüe. We are very grateful to the following agencies and organizations for financial support:

Argentina – Comisión Nacional de Energía Atómica; Agencia Nacional de Promoción Científica y Tecnológica (ANPCyT); Consejo Nacional de Investigaciones Científicas y Técnicas (CONICET); Gobierno de la Provincia de Mendoza; Municipalidad de Malargüe; NDM Holdings and Valle Las Leñas; in gratitude for their continuing cooperation over land access; Australia – the Australian Research Council; Belgium – Fonds de la Recherche Scientifique (FNRS); Research Foundation Flanders (FWO); Brazil – Conselho Nacional de Desenvolvimento Científico e Tecnológico (CNPq); Financiadora de Estudos e Projetos (FINEP); Fundação de Amparo à Pesquisa do Estado de Rio de Janeiro (FAPERJ); São Paulo Research Foundation (FAPESP) Grants No. 2019/10151-2, No. 2010/07359-6 and No. 1999/05404-3; Ministério da Ciência, Tecnologia, Inovações e Comunicações (MCTIC); Czech Republic – Grant No. MSMT CR LTT18004, LM2015038, LM2018102, CZ.02.1.01/0.0/0.0/16_013/0001402, CZ.02.1.01/0.0/0.0/18_046/0016010 and CZ.02.1.01/0.0/0.0/17_049/0008422; France – Centre de Calcul IN2P3/CNRS; Centre National de la Recherche Scientifique (CNRS); Conseil Régional Ile-de-France; Département Physique Nucléaire et Corpusculaire (PNC-IN2P3/CNRS); Département Sciences de l'Univers (SDU-INSU/CNRS); Institut Lagrange de Paris (ILP) Grant No. LABEX ANR-10-LABX-63 within the Investissements d'Avenir Programme Grant No. ANR-11-IDEX-0004-02; Germany – Bundesministerium für Bildung und Forschung (BMBF); Deutsche Forschungsgemeinschaft (DFG); Finanzministerium Baden-Württemberg; Helmholtz Alliance for Astroparticle Physics (HAP); Helmholtz-Gemeinschaft Deutscher Forschungszentren (HGF); Ministerium für Kultur und Wissenschaft des Landes Nordrhein-Westfalen; Ministerium für Wissenschaft, Forschung und Kunst des Landes Baden-Württemberg; Italy – Istituto Nazionale di Fisica Nucleare (INFN); Istituto Nazionale di Astrofisica (INAF); Ministero dell'Universitá e della Ricerca (MUR) ; CETEMPS Center of Excellence; Ministero degli Affari Esteri (MAE), ICSC Centro Nazionale di Ricerca in High Performance Computing, Big Data

and Quantum Computing, funded by European Union NextGenerationEU, reference code CN_00000013; México – Consejo Nacional de Ciencia y Tecnología (CONACYT) No. 167733; Universidad Nacional Autónoma de México (UNAM); PAPIIT DGAPA-UNAM; The Netherlands – Ministry of Education, Culture and Science; Netherlands Organisation for Scientific Research (NWO); Dutch national e-infrastructure with the support of SURF Cooperative; Poland – Ministry of Education and Science, grants No. DIR/WK/2018/11 and 2022/WK/12; National Science Centre, grants No. 2016/22/M/ST9/00198, 2016/23/B/ST9/01635, 2020/39/B/ST9/01398, and 2022/45/B/ST9/02163; Portugal – Portuguese national funds and FEDER funds within Programa Operacional Factores de Competitividade through Fundação para a Ciência e a Tecnologia (COMPETE); Romania – Ministry of Research, Innovation and Digitization, CNCS-UEFISCDI, contract no. 30N/2023 under Romanian National Core Program LAPLAS VII, grant no. PN 23 21 01 02 and project number PN-III-P1-1.1-TE-2021-0924/TE57/2022, within PNCDI III; Slovenia – Slovenian Research Agency, grants P1-0031, P1-0385, I0-0033, N1-0111; Spain – Ministerio de Economía, Industria y Competitividad (FPA2017-85114-P and PID2019-104676GB-C32), Xunta de Galicia (ED431C 2017/07), Junta de Andalucía (SOMM17/6104/UGR, P18-FR-4314) Feder Funds, RENATA Red Nacional Temática de Astropartículas (FPA2015-68783-REDT) and María de Maeztu Unit of Excellence (MDM-2016-0692); USA – Department of Energy, Contracts No. DE-AC02-07CH11359, No. DE-FR02-04ER41300, No. DE-FG02-99ER41107 and No. DE-SC0011689; National Science Foundation, Grant No. 0450696; The Grainger Foundation; Marie Curie-IRSES/EPLANET; European Particle Physics Latin American Network; and UNESCO.